Aeolian Research 17 (2015) 49–60

Contents lists available at ScienceDirect

Aeolian Research

journal homepage: www.elsevier.com/locate/aeolia

Formation of gravel-mantled megaripples on Earth and Mars: Insights from the Argentinean Puna and wind tunnel experiments

N.T. Bridges [a,*], M.G. Spagnuolo [b,1], S.L. de Silva [b], J.R. Zimbelman [c], E.M. Neely [b,d]

[a] Johns Hopkins University Applied Physics Laboratory, Laurel, MD 20723, United States
[b] Oregon State Univ., Corvallis, OR 97331, United States
[c] CEPS/NASM, Smithsonian Institution, Washington, DC 20013-7012, United States
[d] Department of Geology, Portland State University, Portland, OR 97201, United States

ARTICLE INFO

Article history:
Received 16 August 2014
Revised 19 January 2015
Accepted 19 January 2015

Keywords:
Ripples
Megaripples
Puna
Mars
Wind tunnel
Threshold

ABSTRACT

Pumice and lithic clasts from gravel-mantled megaripples in the Argentinean Puna, an analog to Martian large ripples and Transverse Aeolian Ridges (TARs), were put in a boundary layer wind tunnel to derive threshold speeds for various stages of motion of the component clasts and observe incipient bedform development. Combined with results from a field meteorological station, it is found that the gravel components can initially only move under gusty conditions, with the impact of saltating pumice and sand lowering threshold. Pumices can saltate without the impact of sand, implying that they are both an impelling force for other pumices and lithics, and are the most likely clast constituent to undergo transport. Accumulation into bedforms in the tunnel occurs when clasts self organize, with larger, more immobile particles holding others in place, a process that is accentuated in the field on local topographic highs of the undulating ignimbrite bedrock surface. In such an arrangement, pumices and especially lithics remain largely stable, with vibration the dominant mode of motion. This results in sand and silt entrapment and growth of the bedform through infiltration and uplift of the gravel. Resulting bedforms are gravel-mantled ripple-like forms cored with fine grained sediment. The Martian aeolian environment is similar to the Puna in terms of having grains of variable size, infrequent wind gusts, and saltating sand, implying that some TARs on the planet may have formed in a similar way.

1. Introduction

The Martian surface contains a diversity of aeolian landforms, attesting to the effectiveness of wind as a major geomorphic agent despite the lower atmospheric pressure, gravity, and frequency of threshold winds compared to Earth. Martian "Transverse Aeolian Ridges" (TARs) have sizes and morphometric properties intermediate between dunes and ripples. They have been proposed as large megaripples formed via impact splash and creep, reversing dunes, or both (Bourke et al., 2003; Balme et al., 2008; Zimbelman, 2010). Unlike many classic dunes and ripples on Mars, TARs are exclusively immobile at the spatial scales (down to 25 cm/pixel) and temporal baselines (7+ years) obtainable from HiRISE (Bridges et al., 2012, 2013). Similarly, it has been inferred that TARs distal to large dunes are inactive under present conditions (Berman et al., 2011). The apparent immobility of TARs may be from armoring by coarse grains like those that characterize smaller plains ripples in Terra Meridiani (Sullivan et al., 2005). Indeed, the superposition relationships of such granule ripples with small craters along the MER Opportunity traverse path indicate that these bedforms have been static for on the order of 10^5 years (Golombek et al., 2010). This may also explain why some Martian large transverse bedforms are aligned, and apparently fixed upon, the crests of periodic bedrock ridges that have been hypothesized to form from aeolian erosion (Montgomery et al., 2012) (Fig. 1).

Martian dunes and sand ripples have fairly close terrestrial morphometric analogs, emphasizing the role of saltation and impact splash in both environments. However, TARs are a class of Martian bedform for which a viable terrestrial comparison is much harder to find. The gravel bedforms (megaripples) fields in Catamarca province, Argentina (Milana, 2009; de Silva, 2010; Milana et al., 2010) are located in one of the windiest parts of the Argentinean Puna and may be the best terrestrial analog for some TARs (de Silva et al., 2013). The gravel megaripples in Wright Valley, Antarctica are also a potential analog, although being of lower wavelength, aspect ratio, and maximum height relative to the Puna bedforms (Gillies et al., 2012). The Puna gravel bedforms

* Corresponding author.
[1] Now at: IDEAN, UBA-CONICET Ciudad de Bs, As., Argentina.

http://dx.doi.org/10.1016/j.aeolia.2015.01.007
1875-9637/

are built on a bedrock of rhyolitic ignimbrites that contain about 10% by volume of lithic clasts with densities ranging from 2600 to 3000 kg m^{-3}, and up to 20% crystal-poor pumice clasts with densities of ~800 to 1300 kg m^{-3}. Currently, fine sand is being actively transported through the region. The distribution of the gravel classes (lithics, pumice, and milky quartz) varies geographically, with ripple fields located within basins bounded by highstanding volcanic materials and metamorphic basement.

In this paper, we use gravel from the Campo Piedra Pomez (CPP), Campo Purulla (CP), Salar de Incahuasi (SI), and White Barchan (WB) ripple fields. Our weather station is deployed in SI. Here we provide a brief review of the lithologies and characteristics of these fields (for a more detailed discussion of these and other Puna ripple field lithologies, the reader is referred to de Silva et al. (2013)). CPP is the largest field and dominated by dark megaripples composed of older ignimbrite and blackish lavas, including those from the Carachi Pampa cinder cone that borders the field to the northeast. The CP field, due west of Cerro Purulla, has ripples composed of reddish-brown gravel from the adjacent Upper Miocene Rosada ignimbrite, white clasts from the local Paleozoic basement, and andesite. The SI field has similar componentry to CP. WB is dominated by milky quartz gravels whose sizes are generally smaller than grains composing the other ripple fields.

Field observations show that the largest Puna gravel-mantled megaripples are closely aligned with the bedrock ridges (Fig. 2), including some sinuous forms that mirror topography found on the ignimbrite surface in exposed areas (Fig. 3). This is in contrast to other megaripples on Earth, such as those in Wright Valley, Antarctica, whose sinuosity seems solely due to transverse instabilities affecting their formation (Gillies et al., 2012). The inter-ripple area is relatively flat lying, variously consisting of ignimbrite bedrock of low surface roughness and a scattering of pumice-dominated particles. Such areas commonly contain smaller ripples that do not appear aligned with topographic ridges and may be in a state of incipient migration (Fig. 3). Sand deposits are completely lacking. Cross sections of megaripples on bedrock ridges show a ~10 cm upper zone dominated by lithic and pumice grains, with the pumices concentrated on the lee side and commonly merging downwind with more scattered gravel in the inter-ripple zone. Beneath lies a 1s to lower of 10s of cm-thick layer of fine-grained sand and silt (<125 μm), below which is the ignimbrite surface (Fig. 5 of de Silva et al., 2013). On any given day in the field, sand can be felt saltating in the lower ~0.5 m above the surface during high wind events. This suggests that, despite the lack of surface deposits, sand is being transported across the field, with a minor component getting trapped among the ripple clasts.

These observations indicate a sequence of events in which (1) strong winds segregate pumice and lithics from the ash, (2) the ripples nucleate on the bedrock ridges, with the low density pumice becoming concentrated in the protective ridge lee, leaving a greater fraction of lithic and external quartz gravel (depending on field location), (3) sand and silt settle in the interstices of the coarser grains, pushing them up in a process analogous to the formation of desert pavement, (4) the ripples become stabilized on the ridges (Figs. 10 and 11 of de Silva et al., 2013), although some limited migration may occur depending on bedrock topography (e.g., gravels are best stabilized on the largest ridges, but may become decoupled from smaller ridges in high wind events). The bedrock-anchored megaripples are therefore not bedforms in the classic sense of being accumulations of aeolian sediment that migrate over time, but rather consist of surface gravel on ridges, with gravel migration from one ridge to the next occurring in high wind events. Some of the transport flux between ridges probably occurs via smaller ripples, commonly oriented sub-parallel to nearly traverse from the main set (Fig. 3).

This and recent studies are just beginning to understand the aeolian geology of this area (Milana, 2009; de Silva, 2010; Milana et al., 2010; de Silva et al., 2013). These investigations have been challenged by the absence of any local long term wind records. Milana (2009) presented some of the first wind data obtained from a mine located 300 km south at a comparable altitude to the gravel-mantled megaripple fields. More recently, wind data were acquired from two meteorological stations located at 25°06′S, 68°20′W (altitude 5200 m), and at 25°03′S, 68°13′W (altitude 4092 m), ~160 km NNE and ~180 km NNE, respectively from the studied area (de Silva et al., 2013). These data, although instructive, are not within the field area and therefore at best only generally bound wind conditions that affect ignimbrite abrasion and the subsequent modification, segregation, and organization of ignimbrite-derived and externally-transported clasts into the megaripples. Variations in wind intensity, gustiness, direction, and temperature, at diurnal and seasonal scales are best assessed via monitoring from a meteorological station in the area of interest. That is done here, as described below.

Until now, there has been a poor understanding of the threshold speeds needed to set the various coarse-grained materials into motion, namely the pumice and lithics clasts, and what effects the role of impacting pumice and sand has on these thresholds. In addition, the mechanisms for the initial clustering of these coarse components into nascent ripples and the effect this has on subsequent migration has not been documented. Such information can be acquired from boundary layer wind tunnel experiments. There is a mature literature on the aeolian thresholds of spherical particles as a function of size and density (Iversen et al., 1976; White et al., 1976; Iversen and White, 1982; Greeley and Iversen, 1985), but no studies (that we are aware of) on wind speeds needed to move clasts of the specific size, density, and shape that we find in the Puna, nor on the initial stages of ripple development for such particles (a recent study on the saltation thresholds of pumice and scoria particles at various bed slopes (Douillet et al., 2014) focuses on the deposition of pyroclastic density currents, a very different application to that here). These results are reported in this paper, compared to current winds measured from a new field weather station, then used to predict conditions for Puna megaripple formation, and finally applied to a model for the formation of large ripples and TARs on Mars. We show that on a relatively flat, low roughness surface equivalent to that for fresh ignimbrite bedrock in the Puna, periodic wind gusts are sufficient to initially saltate pumice and some lithic clasts and concentrate them into ripples where they remain largely stable, except for rare pumice saltation under very high speed winds and periodic vibration of clasts, which allows sand and silt to infiltrate the ripple interior. Pumices, in addition to saltating on their own, can act to impel other pumices and lithics. Such high winds gusts are reached in the Puna, showing that current conditions can form the ripples. Mars, although differing in the specifics of particle and environmental conditions, has an analogous combination of variable particle sizes, saltating sand, rare gusts, and an ample supply of dust such that large ripples and TARs can likely form in a similar way to that in the Puna.

2. Methods

2.1. Wind tunnel

The boundary layer wind tunnel at Arizona State University was used to study ripple formation, threshold stages, and freestream threshold speeds of Puna materials. It operates at standard pressure and temperature, with a fan and motor system able to achieve freestream winds up to 30 m s^{-1}. It has dimensions of 9.4 m

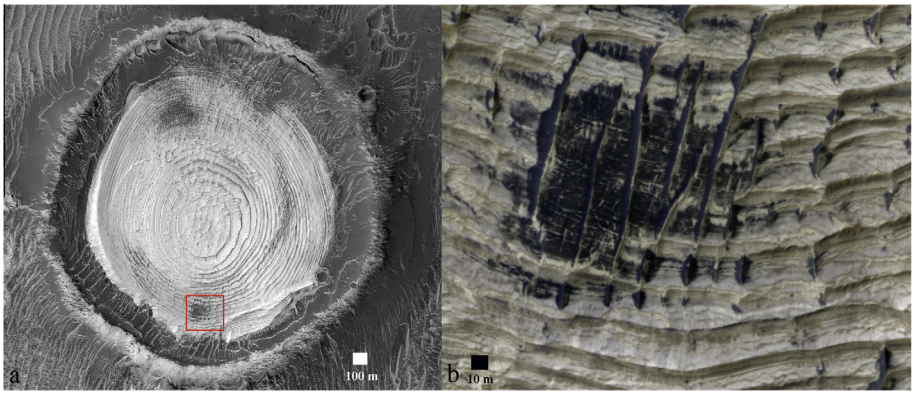

Fig. 1. Nucleation of sand onto bedrock ridges on Mars. (a) A portion of HiRISE image ESP_032836_1790 (in HiRISE's red monochrome channel), of a crater in Schiaparelli basin. Within the crater are circumferential terraces overlain by NNE-SSW-trending ridges. The red box demarcates the location of the enlargement in (b). (b) Close-up of the ridges (seen in the portion of the HiRISE image with color data). Here, dark sand has nucleated onto the ridges. This is similar to the nucleation of material on ignimbrite ridges in the Puna and, as shown in the wind tunnel, the clumping of clasts that develop into ripple-like forms (Fig. 9). (For interpretation of the references to color in this figure legend, the reader is referred to the web version of this article.)

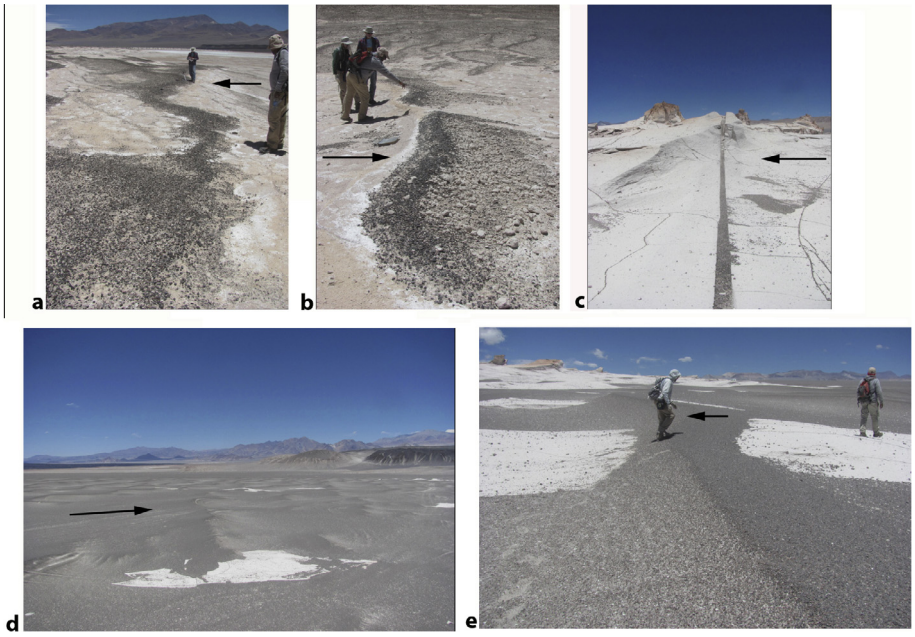

Fig. 2. Bedrock ridges and alignment of megaripples in the Puna. Arrows show the direction of the strongest winds (pointing downwind) inferred from ripple and bedrock geometry: (a) Gravels organized into megaripples and aligned on bedrock ridges near the Laguna Purulla (LP) field, (b) close-up of LP megaripples; note the concentration of pumices on the lee (right) side of the bedforms, (c) Bedrock near the White Barchan field, shown in an area of limited gravel to demonstrate how the ridges form. The crack is where hot gasses escaped through the cooling ash, hardening the ignimbrite relative to the surrounding rock. Subsequent aeolian abrasion has left the harder areas as higher standing ridges, commonly aligned with yardang heads as seen here. (d) WB megaripple field, with some exposed bedrock, (e) close-up of a WB megaripple.

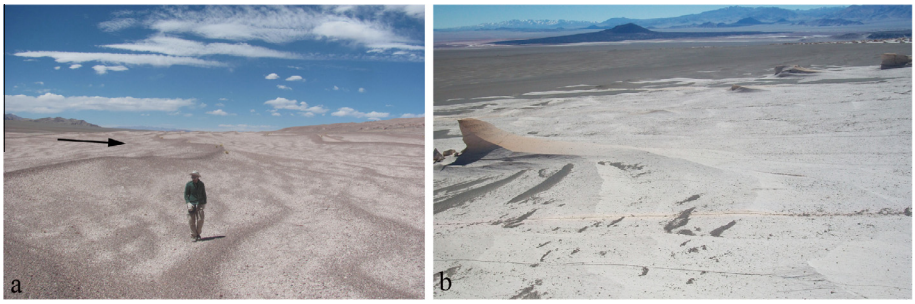

Fig. 3. (a) Megaripples and smaller inter-ripples in the Campo Purulla field. The arrow shows the direction of the strongest winds (pointing downwind) inferred from ripple geometry, which also corresponds to the maximum winds measured with the meteorology station (Fig. 11). The position of the megaripples is influenced by bedrock topography whereas the smaller ripples are likely transporting clasts from one megaripple to the next. (b) An example of uncovered sinuous bedrock ridges on the ignimbrite surface near the northeast margin of the Campo Piedro Pomez field (~28 km ENE from Campo Purulla). Such topography underlies the ripple fields, serving as gravel nucleation sites and thereby influencing the position of the primary ripple sets.

(length from back of roughness elements to fan) × 1.0 m (width) × 0.8 m (height). A motorized hopper can drop sand at variable fluxes. Instrumentation associated with the wind tunnel includes pressure and temperature sensors, wind velocity probes, and humidity monitors. The test section consists of Plexiglas on the side and top, allowing documentation from a range of vantage points. The test section floor is coated with 120 μm (mean) glued sand. Upwind of the sandpaper the surface is smooth plywood.

Prior to the threshold experiments, boundary layer profiles were measured to calibrate the wind tunnel against previous runs using the ASU facility. Based on these, it was verified that free-stream (u_∞) is reached at the fixed pitot height of 36 cm above the wind tunnel floor. Ripple components collected in the field were placed in the tunnel test section. For experiments simulating the impact of saltating particles, quartz sand (Silver Sand #30, PW Gillibrand) was placed in the overhead hopper and dropped into the wind stream. Sunset Crater scoria, a proxy for impacting pumice, at 800 μm average diameter, was too large to feed through the hopper, so was placed upwind of the test section in an unconsolidated pile that was blown downwind at a progressively greater flux as wind speed increase. An overhead still camera took pictures with a 1-min cadence over the experiment duration. Side-mounted video and still pictures downwind and above the wind tunnel floor viewed the runs in perspective. Wind speed was gradually ramped up from zero and stages of particle motion (vibrating, sliding, rolling, and saltating) as a function of composition and approximate size noted in recorded voice cues. Qualitative spoken notes on experiment behavior, such as the clumping and distribution of ripples, movement of particular clasts, etc., were made.

The experimental matrix consisted of 6 samples from the Campo Purulla (GD-010-006, GD-010-007), Campo Piedra Pomez (GD-010-004), Laguna Purulla (GD-010-005), and White Barchan (GD-010-001, GD-010-002) ripple fields (Tables 1 and 2). Out of these samples, three classes of particles at a range of sizes were used: Coarse (2–8 cm) pumice from CP, LP, and WB; coarse lithics (0.5–3 cm) from all four areas; quartz gravels and sand from WB. The pumices and lithics, with the largest sizes, were the most easily documented and are the focus of the results reported here. Materials were variously distributed upwind of the test section on the wood floor, and within the test section upwind and downwind of the pitot tube (Table 1, Fig. 4). The various mixing

Table 1
Experiment summary.

Experiment	Threshold type	Impacting material	Impacting material feed source	Floor Materials (sample ID, field location)	Wind tunnel placement	Floor materials (type [size range])	Duration (min:s)
P-12-005	Fluid	NA	NA	GD-010-005 (CP)	1, 2	Lithics (*coarse*), pumice (*coarse*)	15:00
P-12-006 (cont. of P-12-005)	Impact	Quartz sand	Hopper	GD-010-005 (CP)	1, 2	Lithics (*coarse*), pumice (*coarse*)	17:00
P-12-007	Fluid	NA	NA	GD-010-002 (WB)	1, 2, 3	Lithics (*coarse*), pumice (*coarse*)	10:45
P-12-008	Fluid	NA	NA	GD-010-004 (CPP)	1, 2, 3	Lithics (*coarse*), quartz (*coarse*)	13:35
P-12-009	Fluid	NA	NA	GD-010-001 (WB)	1, 2	Quartz sand	15:05
				GD-010-006 (CP)	1, 3	Pumice (*coarse*)	
P-12-010	Impact	Quartz sand	Hopper	GD-010-002 (WB)	1, 2	Lithics (*coarse*), pumice (*coarse*)	16:20
				GD-010-006 (CP)	3	Pumice (*coarse*)	
P-12-011 (cont. of P-12-010, with GD-010-007 added)	Impact	Scoria	Upwind floor	GD-010-002 (WB)	1, 2	Lithics (*coarse*), Pumice (*coarse*)	9:30
				GD-010-006 (CP)	3	Pumice (*coarse*)	
				GD-010-007 (SI)	3	"Gravel" (*coarse*)	
P-12-012	Impact	Scoria	Upwind floor	GD-010-002 (WB)	1, 2	Lithics (*coarse*), pumice (*coarse*)	10:46
				GD-010-007 (SI)	3	"Gravel" (*coarse*)	
				GD-010-005 (LP)	3	Lithics (*coarse*), pumice (*coarse*)	
P-12-013	Impact	Scoria	Upwind floor	GD-010-006 (CP)	2	Pumice (*coarse*)	13:55
				GD-010-007 (SI)	2, 3	"Gravel" (*coarse*)	
				GD-010-005 (LP)	2, 3	Lithics (*coarse*), pumice (*coarse*)	
P-12-014 (cont. of P-12-013)	Impact	Scoria	Upwind floor	GD-010-006 (CP, ripple lee)	2	Pumice (*coarse*)	15:20
				GD-010-007 (SI)	2, 3	"Gravel" (*coarse*)	
				GD-010-005 (CP)	2, 3	Lithics (*coarse*), pumice (*coarse*)	

Ancillary notes:
CP = Campo Purulla, CPP = Campo Piedra Pomez, LP = Laguna Purulla, WB = White Barchan.
Wind tunnel placement: 1: Upwind of test section, 2: Test section upwind of pitot tube; 3: Test section downwind of pitot tube.
P-12-005: Coarse gravel distributed upwind of pitot, about 1 clast thick; 10 cm gap between material and walls.
P-12-006 uses GD-010-005 materials left over from P-12-005.
P-12-007: Individual clasts put upwind and downwind of patch to see any if there were any effects of roughness differences; one 1 cm pumice clast to the left of the FOV.
P-12-008: Line of clasts put in upwind and downwind.
P-12-009: Quartz sand placed in elongated patch upwind of traversing pitot; 5 large pumices placed upwind of quartz batch, on either side (3 on nearside, 2 on farside); 9 pumices placed 1.5 m downwind from pitot, in a row.
P-12-010: The Campo Purulla pumice consisted of 6 large clasts placed downwind from White Barchan samples.
P-12-011: About 1/2 bucket of Sunset Crater scoria placed below hopper feed on tunnel floor; in test section were remnant materials from P-12-010 (including one big pumice in same position and orientation) and some GD-010-007 gravel downwind; only about 10% of the scoria was used in the experiment.
P-12-012: Remnants of 1/2 bucket from P-12-011 plus another 1/2 bucket (so ~95% of a full bucket) of Sunset Crater scoria were placed below hopper feed on tunnel floor.
P-12-013: Full bucket of Sunset Crater scoria placed below hopper feed on tunnel floor; test section materials (GD-010-007; GD-010-005) are distributed farther apart than in P-12-012.

Table 2
Experiment material locations.

Field (sand)	Location	Landform	Lithics (coarse)	Pumice (coarse)	Quartz (coarse)	Quartz
Campo Piedra Pomez						
GD-010-002	26°34′58.81″S, 67°28′15.08″W	Bedform crest	X	X		
Campo Purulla						
GD-010-005	26°36′44.11″S, 67°46′19.89″W	Bedform lee	X	X		
GD-010-006	As above	Bedform lee		X		
Salar de Incahuasi						
GD-010-007	26°36′45.74″S, 67°46′16.42″W	Bedform crest	X			
White Barchan						
GD-010-001	26°35′58.79″S, 67°26′40.08"W	Bedform crest				X
GD-010-004	26°35′58.79″, 67°26′39.99″W	Whole bedform		X	X	

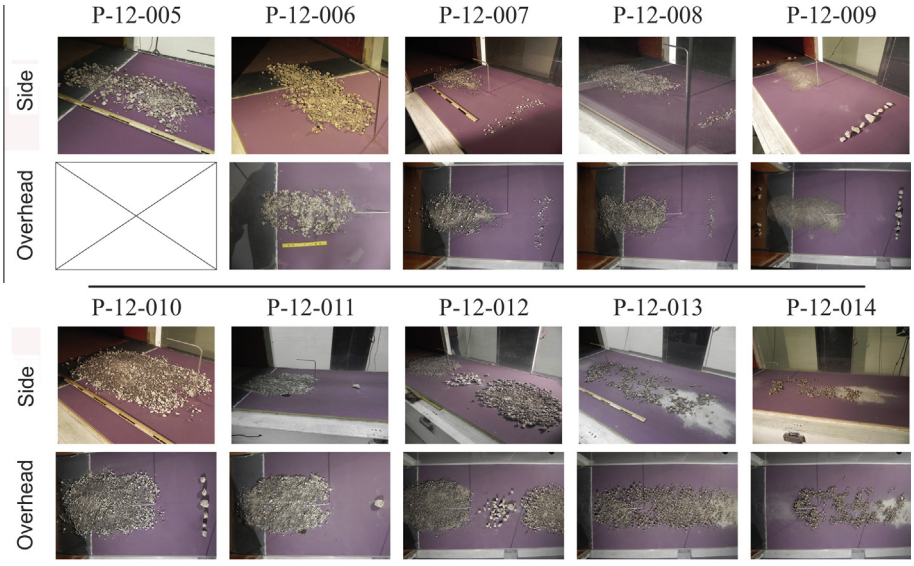

Fig. 4. Side and overhead views of the wind tunnel experiments at the start of each run.

and arrangement of materials simulates aspects of the field environment in regard to determining threshold, namely:

(1) The size, shape, and density of sand and gravel, as these are field samples.
(2) Surface roughnesses ranging from the nearly perfectly smooth wood floor, to the sandpaper, to particles surrounded by others of various sizes. Although the aerodynamic roughness heights (z_0) are not known, they can be estimated. The wood floor is considered nearly perfect smooth, with $z_0 < 1$ μm. The sandpaper grains are approximately spherical and equally spaced, such that z_0 is ideally ~1/30th the grain diameter (Bagnold, 1954) of 120 μm (mean), corresponding to a roughness height of 4 μm. The mixed particles should have roughnesses dominated by the larger gravels that shelter the smaller ones, so z_0s of millimeters to ~1 cm. The first two cases span the range of roughnesses on the level areas of the ignimbrite surface. They therefore apply to pre-ripple stages in which particles are variously distributed on the surface, and current conditions where grains are located between ripples, and the upwind boundary of ripples that border the ignimbrite. The last case best simulates the arrangement of grains on a gravel ripple surface.
(3) The effect of saltating particles in lowering threshold of larger clasts. Four of the ten experiments were run under pure fluid conditions, that is, with the only pre-threshold forces on the particles being lift and drag from the wind. The other six had quartz sand and scoria impacting the particles, as described above. These two cases are qualitatively labeled here as "fluid" and "impact" threshold, although the conditions differ from the classic definitions from which quantitative results are derived (e.g., Kok et al., 2012). For the fluid case, the particle sizes, shapes, and densities, and the surface roughnesses, were mixed. Although representing many aspects of field conditions, threshold results for a specific particle differs from the ideal case in which all other particles are identical and perfectly geometrically arranged. Impact threshold is traditionally defined as the change in freestream wind speed (or friction speed or shear stress) resulting from the more efficient (in the case of Earth and Mars) transfer of momentum from impacting particles to splashed grains in the bed (Ungar and Haff, 1987; Andreotti, 2004; Kok, 2010; Kok et al., 2012). The wind tunnel results should therefore be considered semi-quantitative data that inform upon and bound field conditions.

The side-mounted videos were analyzed using Kinovea software from which particle motion was tracked. For all clasts >0.3 cm that eventually attained motion, the area within an enclosed polygon around each clast was measured, and then the effective diameter calculated by the software from the number of pixels subtended at a given scale. This allowed the correlation between the stages of motion (vibrating, sliding, rolling, and saltating) to size as a function of composition and location. The onset of

the stages of motion for these clasts were compiled for lithic and pumice. The motion stages were also correlated to a freestream wind speed by comparing the video chronometer to the time-tagged pitot record. Size as a function of composition was plotted against freestream wind speed and fitted to regression lines to get approximate threshold curves.

2.2. Field meteorological station

The station was placed in the Salar de Incahuasi field (26°28′58.6″S, 67°41′1.3″W; 3322 m) spaced more than 7 m from ~1 m high megaripples to the southeast and northwest, with NE-SW being approximate corridors between these bedforms (Fig. 5). The local surface roughness is dominated by cm-scale pumice and lithic clasts, with some larger pumices of 10s of cm size. In the megaripple inter-areas, where the station is located, the pumice and lithics are approximately segregated into clumps that resemble ripples in planview but have no discernable topographic profile (background of Fig. 5). The wind sensor is located 1.6 m above the ground. Wind ripple profiles show that the inter-megaripple troughs, including the location of the station, are not influenced by boundary layer separation as is the case nearer the megaripples (Zimbelman et al., 2014). Therefore, the profiles and roughnesses should correlate to the troughs and the upwind portion of megaripples. Average wind speed and peak gust, and temperature, were recorded every 30 min from March 30 to November 17, 2013.

3. Results

3.1. Wind tunnel

As the freestream wind speed in the tunnel increased, most particles transitioned through progressive stages of motion from their initial static state:

(1) Vibrating: Grains oscillated back and forth from an anchored pivot point, generally along one axis of motion.
(2) Sliding: Particles slid along the surface, usually in a constant direction.
(3) Rolling: Grains rotated about an approximately fixed axis and migrated downwind.

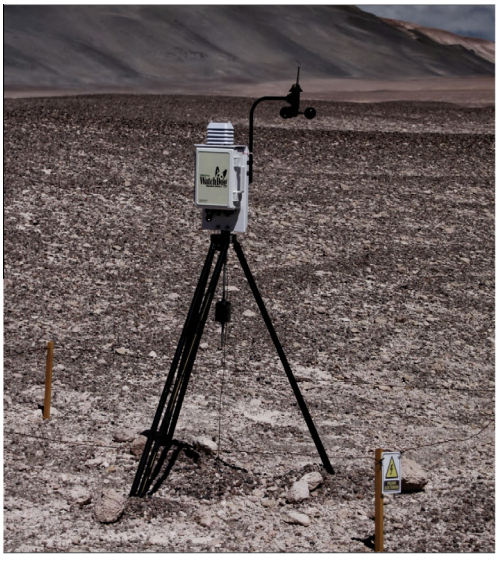

Fig. 5. Autonomous meteorological station in the Salar de Incahuasi ripple field.

(4) Saltating: Particles hopped off the surface along a ballistic trajectory.

Whether particles underwent motion, the final stage reached if they did, and the freestream wind speed at each transition depended on four primary factors: (1) The position of the grain relative to others (either on the edge of a patch of clasts or within the patch; subsequently referred to as "edge" and "patch" data, respectively), (2) the material density as reflected in the composition, (3) size, and (4) whether or not the particles were impacted by saltating grains, and the composition (quartz sand vs. scoria) of these impactors. These qualitative transitions observed and recorded in the videos can be semi-quantified by reducing the data as described in the previous section and displaying in a series of plots. We consider these results "semi-quantitative" in that the experiments contain a range of particle sizes, shapes, and densities variously distributed across different roughness surfaces and, as such, differ from classic threshold experiments in which conditions were finely tuned (Iversen et al., 1976; White et al., 1976; Iversen and White, 1982). However, they constrain conditions seen in the field.

The transitions show clear dependence on whether or not the particles were impelled by fluid forces only vs. those being impacted by saltating quartz sand and scoria, with quartz sand- and especially scoria-impacted grains showing the greatest number of advanced stages, rolling and saltating (Fig. 6). In addition to the lower threshold for scoria and quartz sand impact-impelled conditions, the stage transitions from vibrating through saltating show a correlation to wind speed, with larger particles generally having greater thresholds.

The data for vibrating clasts shows considerable scatter (Fig. 7). This is in contrast to the trends for saltating grains that will be described below, in which threshold speed is roughly proportional to size. This can be explained by the different physics driving vibration vs. detachment. In the vibration case, the clasts are likely jostled about one or more pivot points, such that even modest winds can induce some vibration. In addition, larger clasts stick higher into the boundary layer where they are subjected to greater aerodynamic force compared to smaller particles. There is therefore some balance between the weight (normal force) and the aerodynamic force that acts to vibrate clasts over a range of sizes. This is in contrast to detachment required for saltation, where the entire particle must be lifted from the surface.

In comparing particle size (average diameter) vs. freestream wind velocity for saltation, several trends and relationships are apparent (Fig. 8). These results are graphed logarithmically, as is common on such plots. In threshold curves for lower particle sizes, the logarithmic slope, m (e.g., u (or u^*) = xd^m) for spherical unconsolidated particles is ~0.5 ($u = xd^{0.5}$), reflecting the balance between the dominant aerodynamic forces and particle weight $(u = (kdg(\rho_p - \rho)\rho)^{0.5} \approx (kdg\rho_p\rho)^{0.5}$, where k is a prefactor that includes particle shape (4/3 for spherical particles) and the drag coefficient, u is wind speed, d is particle diameter, ρ_p is particle density, and ρ is atmospheric density. The results here have shallower slopes, indicating that lower wind speeds are needed to move these particles into saltation compared to the idealized case. As seen in the position of the points, and in the value of the power law pre-factor, x, lithics generally have higher thresholds than pumice, as would be expected given their greater density (~2600 kg m^{-3} vs. 1000 kg m^{-3}). For the edge materials, the ratio of the pre-factors for lithics and pumice in the quartz sand and scoria impact cases are 15/8.6 = 1.7 and 12/9.6 = 1.3. For fluid, there is only one lithic data point, at u = 21.6 m s^{-1} and d = 2.6 cm. Assuming the same 0.18 power law slope as the pumices, the lithic pre-factor is 18.2 ($21.6/2.55^{0.18}$), given a lithic/pumice pre-factor ratio of 18/15 = 1.2. These three ratios are close to the value of the square root of material densities ($(2600/1000)^{0.5}$ = 1.6) as predicted

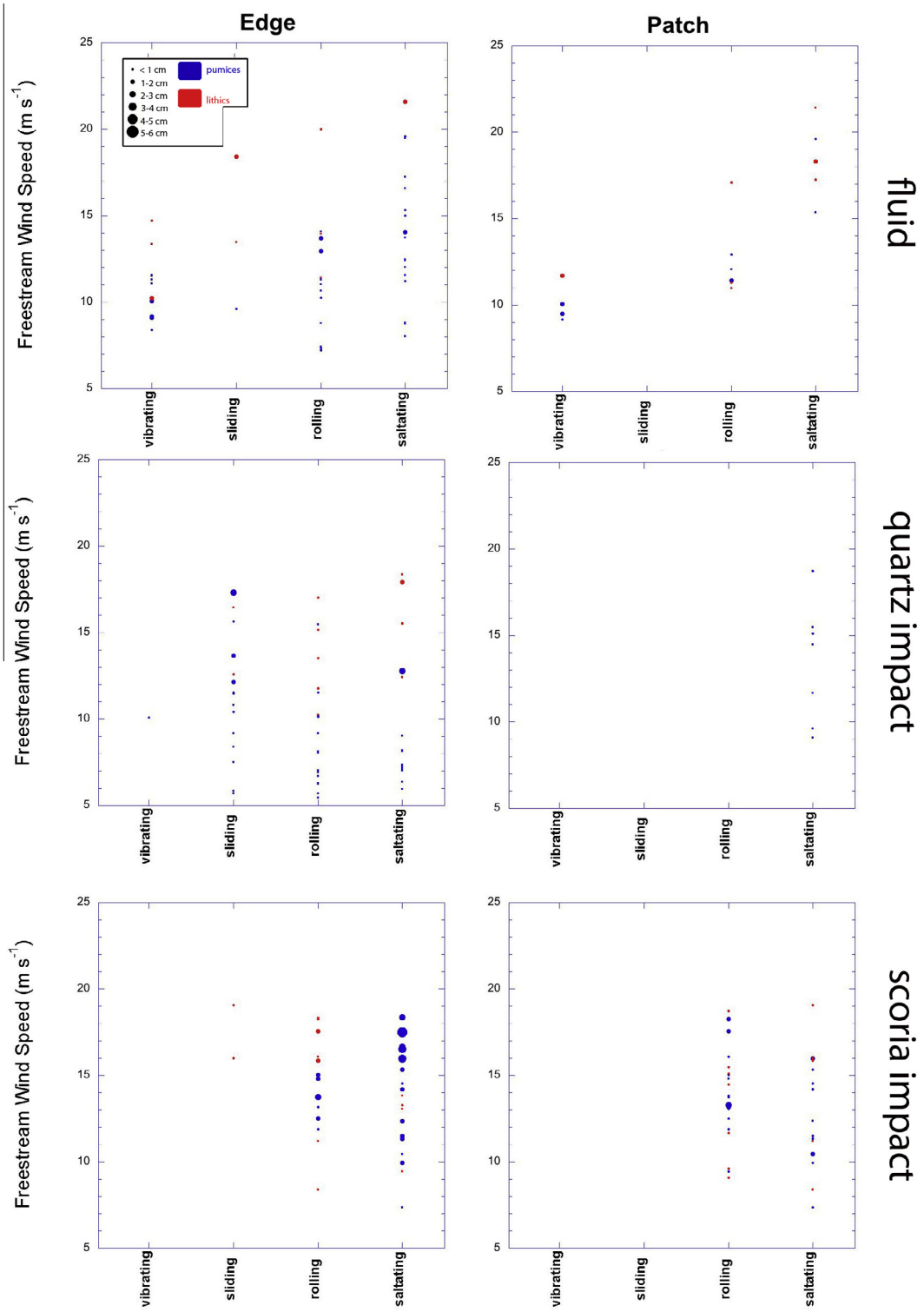

Fig. 6. Stages of motion for pumice samples in the wind tunnel for "fluid," quartz sand impact, and scoria impact conditions. Results are shown for materials on the edges and within patches (clumps) of clasts. The colors refer to pumice and lithic clasts. The sizes of the symbols is proportional to the relative size of the clasts. Velocities are those in Tempe, AZ. Because of the lower atmospheric density in the Puna, wind speeds there would be 1.3× greater than shown here.

by theory. The patch materials, protected from the wind force and particle impact by surrounding clasts, do not show such clear relationships. Fluid thresholds are greater than those for quartz sand and scoria impact. There is no appreciable difference for saltation threshold between scoria and quartz sand impact. The saltation thresholds on the edge are appreciably lower than those within patches. These plots show some scatter, with fairly low R^2 regressions. This can be attributed to the variable clast shape, somewhat random placement in the wind tunnel, and a limited sample size (n) in several cases. For example, the patch lithic data show decreasing slopes, an anticorrelation that is probably best explained by the somewhat random movement of these gravels

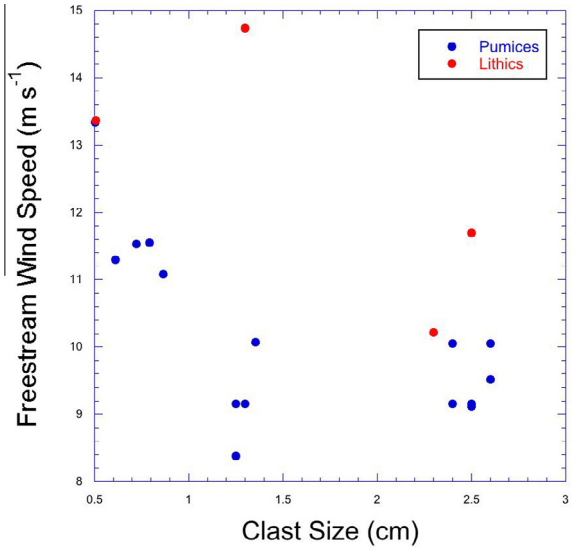

Fig. 7. Freestream wind speed vs. clast size at the vibration stage for all analyzed experiments. The data are scattered, reflecting that factors such as clast shape and position relative to other clasts can affect vibration threshold. Nevertheless, the heavier lithics generally have greater thresholds than the lighter pumices.

caused by the surrounding clasts shadowing and altering the general wind flow in unpredictable ways. As such, these results should not be interpreted as calibrated threshold curves that can be extended to smaller particles sizes where the grains are ideal spherical particles, but rather as semi-quantitative data to inform on field conditions.

As wind speed ramped up, particles tended to self-organize, beginning with uneven clumps that gradually transitioned into elongated forms with their long axes oriented transverse to the wind and exhibiting a ripple-like planform (Fig. 9). The details of this process are seen in the videos. Because smaller particles generally reached threshold stages at lower wind speeds than larger clasts, they tended to slide or roll against stationary or vibrating bigger grains. These grains then clumped against the larger ones, with those that reached the back of the larger grains serving to anchor them in place. Through this gradual process, nascent ripples developed on the wind tunnel floor.

3.2. Field meteorological station

The data from the field meteorological station showed variable daily average and peak gusts from the March to November (2013) time period over a range of 1–29 and 11–90 km h^{-1}, respectively (Fig. 10). The highest speed winds were in the spring, although each month from April through November had days in which averages and gusts were at or exceeded 20 and 59 km h^{-1}, respectively. Rose diagrams of wind directions as a function of season and speed show that all winds and gusts (i.e., >0 km h^{-1}) exhibit a northwesterly and southwesterly flow, with winds >5 km h^{-1} up to gusts >45 km h^{-1} showing mostly northwesterly trends (Fig. 11), consistent with the observed ripple orientation.

4. Interpretations

The wind tunnel data are only relevant to natural conditions if their results can be applied to the field site in the Puna and, given the goals of this overall project, Mars. The main differences between the tunnel and environmental conditions is the atmospheric density (ρ) and, in the case of Mars, gravity (g). The physical surface roughness in the tunnel, as discussed above, varies from smooth plywood to 120 μm glued sand to that induced from the materials themselves. Therefore the aerodynamic roughness, and thus the translation from shear stress to freestream at threshold, is variable and undefined. We thus express our results in terms of freestream wind speed only, and adjust for the other variables by $((\rho_p - \rho)g/\rho)^{0.5}$, in other words, the balance between aerodynamic drag and lift forces vs. gravity. This simple relation holds true for threshold curves above the minimum particle size, below which interparticle forces and Reynolds number effects can dominate (White, 1986). For the Puna, we need only adjust for the atmospheric density. Taking the average Puna elevation of 4500 m and Tempe, AZ as 400 m, and an atmospheric scale height of 8 km, the Puna air densities will be $\exp(-(4.5 - 0.4)/8) = 0.6\times$ that in the wind tunnel assuming equivalent temperatures. The

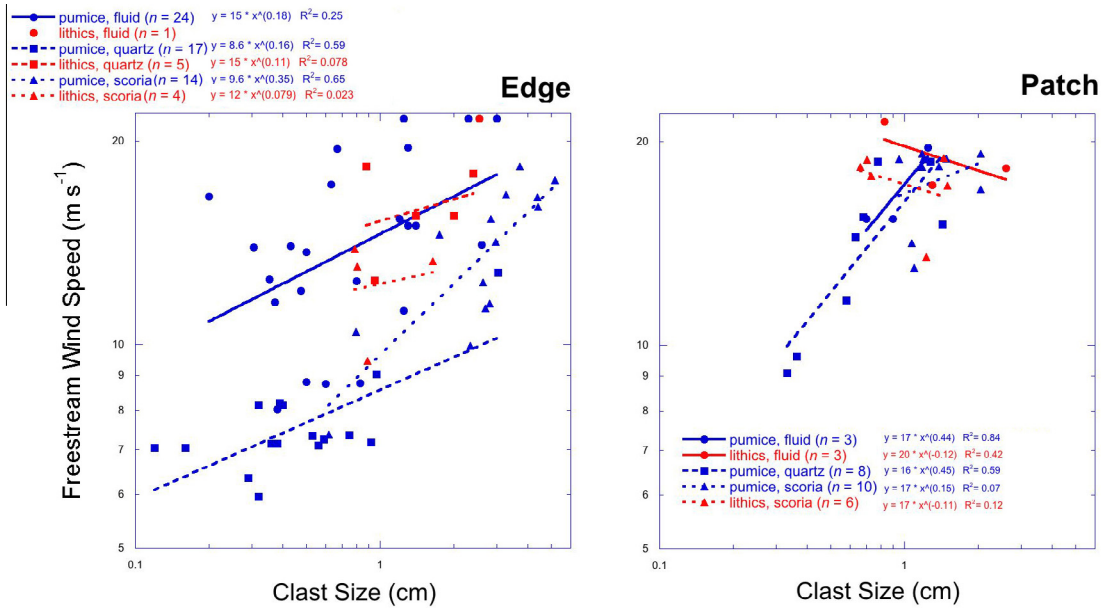

Fig. 8. Freestream threshold wind speeds of pumice and lithic clasts as a function of size as determined in the wind tunnel for "fluid," quartz sand impact, and scoria impact conditions. Results are shown for materials on the edges and within patches (clumps) of clasts. Data are fitted to power laws ($u = xd^m$). The number of data points is indicated by n. Because of the lower atmospheric density in the Puna, wind speeds there would be 1.3× greater than shown here.

Fig. 9. An example of initially scattered clasts (top) clumping of materials into nascent ripples (bottom). In this experiment (P-12-013) pumices and lithics were impacted by scoria particles. The time difference between the two images is 26 min. In this experiment, wind speed was gradually ramped up to 22 m s^{-1}.

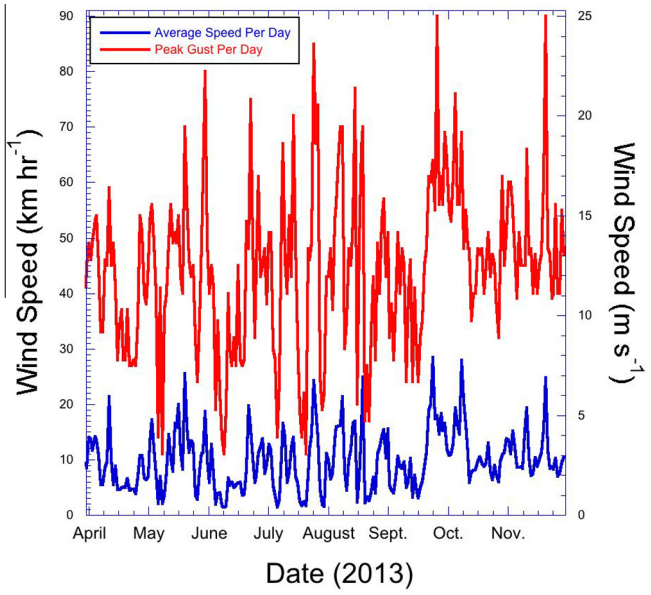

Fig. 10. Average and peak wind gust speeds per day at a height of 1.6 m, from March 30 to November 19, 2013 as measured at the Salar de Incahuasi meteorological station.

wind speeds therefore must be $(1/0.6)^{0.5} = 1.3\times$ greater for an equivalent force. We overlay the wind tunnel minimum vibration and 1 cm clast size saltation thresholds adjusted to Puna conditions onto the field station data in Fig. 12. The thresholds are presented as gradational zones given the variability in the wind tunnel results and field conditions. Despite these approximate boundaries several results are clear. First, average winds do not move the clasts in any mode (i.e., vibration through saltation), with gusts required to exceed threshold. Clasts will vibrate under gusts that occur throughout the year. Similarly, under impact threshold (generally from saltating pumice), pumices at the edges of clast groupings will saltate in typical gusty conditions, with lithic threshold only exceeded a few times per year. If impacting particles are lacking, then pumices and lithics saltate much less frequently. When concentrated within patches, pumices and lithics saltate rarely under impact threshold and for fluid conditions, only pumice saltates, with lithics never moving. This model is conceptual, and other factors must modify these relationships to some extent. For example, the topography of the megaripples will influence wind flow, with shear stress higher on the stoss crest (from the compressing of streamlines) and possible flow detachment, depending on the height and profile, in the lee. This and other factors are avenues for future research.

On Mars, most sand and granules are made of basalt. With a density of 3000 kg m^{-3} and given that the Martian gravity is a factor of 0.37 that on Earth, the weight (*mg*) of basalt on Mars is equivalent to pumice on Earth (e.g., 3000 * 0.37 = 1100). In Terra Meridiani, many granule ripples, which can be considered smaller versions of TARs, also contain clasts of specular hematite (Christensen et al., 2004; Squyres et al., 2004; Weitz et al., 2006). With a density of ~5260 kg m^{-3}, it's weight on Mars is equivalent to materials with a density of ~1950 kg m^{-3} on Earth, so in between the pumice and lithics (~2600 km m^{-3}). Therefore, our results give insight on processes for basalt (pumice equivalent weight) and somewhat for a system with two density components, as at Terra Meridiani. The density of CO_2, the major constituent of the Martian atmosphere, is 0.015 kg m^{-3} at 6.1 mb and 209 K. This compares to 0.71 kg m^{-3} for air at 293 K at 4500 m elevation in the Puna. Therefore, wind speeds must be $(0.71/0.015)^{0.5} = 6.8\times$ greater on Mars to move materials of equivalent weight on Earth, all other conditions being equal. The Martian-equivalent wind speeds are shown in red on the right axes of the plots in Fig. 12. Whether threshold is exceeded on Mars depends on location and season. For example, in the most extreme case on the planet, global circulation models predict that peak noontime winds on Olympus Mons can reach friction speeds of 3.0 m s^{-1} (Newman, personal communication, 2014), about 1.5× the minimum threshold friction speed on Mars (Greeley and Iversen, 1985). However, in general winds exceeding threshold are far more rare on Mars compared to Earth. For example, data from the Viking Landers show that threshold was rarely exceeded, with only minor surface changes seen in more than 6 years of operation at VL1 (Arvidson et al., 1983; Moore, 1985; Almeida et al., 2008). Under such conditions, the coarse materials here would never saltate and only occasionally vibrate on Mars.

5. Discussion

The wind tunnel and weather station results support the sequence of Puna megaripple formation as previously proposed (de Silva et al., 2013) and reviewed in the Introduction. The most important observations are:

(1) Gusts are required to move the clasts when they are exposed to the oncoming wind, with saltating grains lowering threshold. This can be considered the initial stage of ripple formation, before dispersed clasts nucleate. Through all stages, pumices act as both saltating grains and impelling tools against other clasts.
(2) Clasts self-organize into ripple-like features. The wind tunnel experiments show that materials tend to clump, thereby shielding less dense and smaller particles in the interior. This shows that materials can clump when moved by intermittent creep, as has been advocated for the formation of gravel megaripples in Wright Valley, Antarctica (Gillies et al.,

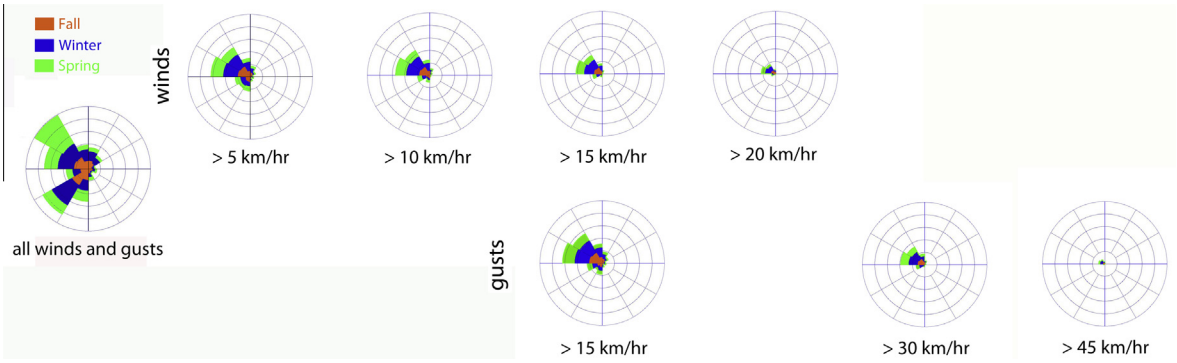

Fig. 11. Rose diagrams showing upwind direction as a function of season and speed as measured from the surface meteorology station from March 30 to November 19, 2013. Each circumferential ring represents 500 events, which were recorded every 30 min.

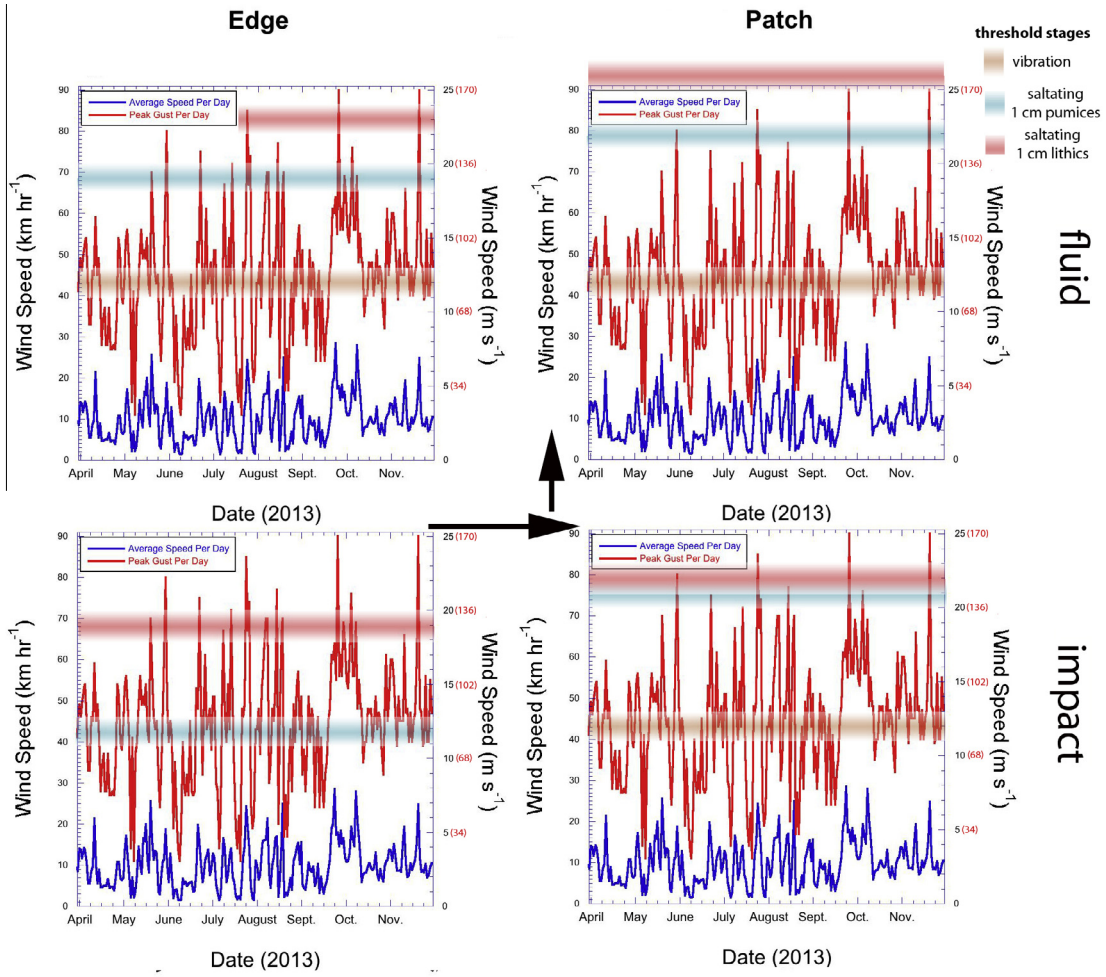

Fig. 12. The Puna wind data from Fig. 10 with overlays of wind tunnel derived freestream thresholds adjusted for the atmospheric density at 4500 m. Wind speeds are shown in units of km h^{-1} on the left axis and m s^{-1} on the right, with Mars equivalent speeds for the same aerodynamic force shown in parentheses in red. The thresholds are shown as gradational given the nature of the wind tunnel experiments and field conditions. The pumice and lithic thresholds are those for 1 cm particles as described in the text and shown in Fig. 8. The impact threshold are centered in the averages for quartz sand and scoria impacts. The vibration threshold is the minimum measured in the wind tunnel experiments and may be greater, depending on the particle size (Fig. 7), and is assumed the same for all cases (it is not shown for the edge impact case to avoid over-plotting on the pumice threshold zone). These results show that saltation, even for pumices, can only occur in gusts at certain times of the year and that once grains are protected within patches, saltation is even more rare. Grains can vibrate through the year, but require gusts. The average daily winds do not modify the surface. The black arrows show the most likely evolutionary path in the development of the Puna gravel-mantled megaripples, beginning with exposed clasts ("edge") being impacted by saltating particles (generally pumices), to clumping of grains ("patch") also exposed to saltating grains, to clumps sufficiently protected that they are sheltered from saltating particles. (For interpretation of the references to color in this figure legend, the reader is referred to the web version of this article.)

2012). Topography can further enhance nucleation and the buildup of clasts, with the largest Puna ripples being located at the crests of pre-existing topographic ridges.

(3) Once nucleated, interior ripple clasts remain fairly stable, with only the strongest gusts moving pumice and rarely, if ever, the lithics. The arrangement is similar to that of the

ripples in the Puna, and the wind tunnel and field wind results show that such "patch" clasts should rarely move (Fig. 12). This is consistent with time-lapse images that recorded some pumice pieces, but no lithics, blown off of ripple crests over a period of 7 months (de Silva et al., 2013). So, despite occasional grains hopping from one ripple to the next in high wind events, the surface is largely stable, with pumices traveling over the surface and impelling other grains.

(4) Gusts continually vibrate pumice and lithics. This explains field observations showing that the cores of the ripples are composed of sand and silt. In this scenario, wind-induced vibration of clasts allows sand and silt to settle among them, resulting in net upward clast movement and the formation of an accreted silt-sand core. Over the long term, this accretion should cause bedform inflation that, combined with further accumulation of gravel, likely accounts for the large scale of the Puna megaripples. It is also likely that the vibrating grains cause not only sand and silt infiltration, but large grains to get jostled into stable positions. Therefore, the longer a clast sits on a ripple, the more stable it gets, such that redistribution decreases and stabilization increases with time.

The applicability to the formation of Transverse Aeolian Ridges on Mars is best considered in terms of process and not as a direct material and size correlation. Although ignimbrites may be present on Mars, such as composing the Medusae Fossae Formation (Scott and Tanaka, 1982; Mandt et al., 2008, 2009), environments containing materials like those in the Puna are probably rare. Nevertheless, much is common on the two planets, such that the results here provide insight on how some TARs could have formed. These commonalities are:

(1) The Martian plains ripples of Terra Meridiani are armored with coarse granules overlying a fine-grained interior (Sullivan et al., 2005). As discussed above, the two density fractions, basalt and the heavier hematite concretions ("blueberries"), are analogous to pumice and lithic clasts in the Puna, with the fine grained interiors of the ripples on both planets similar in terms of grain size.
(2) Example of large TARs superposed on topographic flanks and smaller ones in swales have been documented on Mars, similar to the geometry in the Puna (de Silva et al., 2013) (Fig. 1).
(3) Large ripples and TARs on Mars appear static (Bridges et al., 2012, 2013).
(4) Wind speeds on Mars rarely or never reach that needed to saltate the coarse grains that cap the Martian ripples. Although the impact threshold speeds needed to sustain saltation on Mars are about 10% of the fluid threshold speeds required for initiation, as opposed to ~80% on Earth (Kok, 2010; Kok et al., 2012; Yizhaq et al., 2014), these low values only apply to grains that can be saltated in the first place, and are therefore most applicable to fine and medium sand. Indeed, this likely explains why many Martian dunes and sand ripples are migrating despite TAR immobility.

These comparisons provide a model for the formation for many of the large ripples and TARs on Mars that are consistent with the current aeolian conditions and particle distributions on the planet. In this scenario, an initially random distribution of particles is sorted by the wind into those that can saltate vs. denser and larger ones whose movement would be mostly restricted to creep and traction along the surface, being impelled by the impact of saltating grains. Large ripples could potentially form via this mechanism alone (e.g., as proposed for the megaripples in Wright Valley, Antarctica (Gillies et al., 2012)). However, pre-existing topography offers natural nucleation sites for megaripple accumulation and growth, as is seen in some areas of the planet (Fig. 1). Then, once accumulated into ripple-like forms, the grains remain largely static, with rare Martian gusts occasionally vibrating the grains, allowing the settling of pervasive dust and some sand among the grains, inflating the bedforms over time.

The model proposed is probably not applicable to all TARs and megaripples on Mars, as other mechanisms are possible depending on the local geology (grain sizes, topography, etc.) and conditions (wind speeds and threshold frequencies, atmospheric density, etc.). However, it is consistent with the current Martian environment, and analogous to what is found in the Puna and the wind tunnel experiments and therefore should be considered as a viable scenario to explain many observations. The model does not require a past climate with a thicker atmosphere and stronger winds to form Martian megaripples and TARs. Rather, a suite of particle sizes, saltating grains, and occasional gusts are sufficient. The ideas presented here offer some simple mechanisms that form analogous bedforms on Earth. These ideas can be tested in a number of ways on current and future Mars spacecraft. For example, assuming successful operation for years into the future under extended missions, repeat images from HiRISE will be able to document whether TARs migrate over longer temporal baselines than so far measured. Otherwise, TARs can still be considered static features at the decadal or longer time scale. Current and future rovers, if able to drive onto a TAR, would be able to trench into its surface, showing whether the stratigraphy is like that seen in the Puna and the smaller Terra Meridiani ripples. If so, the formation mechanism proposed here would remain a viable hypothesis.

Acknowledgements

We are indebted to several individuals whose assistance made this project possible. D. Ball, C. Bradbury and A. Zink assisted in the setup, running, and documentation of the wind tunnel experiments. Discussions with R. Sullivan on the wind tunnel and fieldwork were illuminating. Support for this project was provided by grant NNX10AP79G (Principal Investigator de Silva) from NASA's Mars Fundamental Research Program.

References

Almeida, M.P., Parteli, E.J.R., Andrade, J.S., Herrmann, H.J., 2008. Giant saltation on Mars. Proc. Natl. Acad. Sci. USA 105, 6222–6226.
Andreotti, B., 2004. A two-species model of aeolian sand transport. J. Fluid Mech. 510, 47–70.
Arvidson, R.E., Guinness, E.A., Moore, H.J., Tillman, J., Wall, S.D., 1983. 3 Mars years – Viking Lander 1 imaging investigations. Science 222, 463–468.
Bagnold, R.A., 1954. The Physics of Blown Sand and Desert Dunes. Dover Publications, Inc., Mineola, NY, 265 p.
Balme, M.R., Berman, D.C., Bourke, M.C., Zimbelman, J.R., 2008. Transverse aeolian ridges (TARs) on Mars. Geomorphology 101, 703–720.
Berman, B.C., Balme, M.R., Rafkin, S.C.R., Zimbelman, J.R., 2011. Transverse Aeolian Ridges (TARs) on Mars II: Distributions, orientations, and ages. Icarus 213, 116–130.
Bourke, M.C., Wilson, S.A., Zimbelman, J.R., 2003. The variability of transverse aeolian ridges in troughs on Mars. In: Lun. Planet. Sci., XXXIV, 2090.
Bridges, N.T. et al., 2012. Planet-wide sand motion on Mars. Geology 40, 31–34.
Bridges, N.T., Geissler, P., Silvestro, S., Banks, M., 2013. Bedform migration on Mars: current results and future plans. Aeolian Res. 9. http://dx.doi.org/10.1016/j.aeolia.2013.02.004.
Christensen, P.R. et al., 2004. Mineralogy at Meridiani Planum from the mini-TES experiment on the Opportunity rover. Science 306, 1733–1739.
de Silva, S., 2010. The largest wind ripples on Earth: comment. Geology 38, e218.
de Silva, S.L., Spagnuolo, M.G., Bridges, N.T., Zimbelman, J.R., 2013. Gravel-mantled megaripples of the Argentinean Puna: a model for their origins and growth with implications for Mars. Geol. Soc. Am. Bull. 125, 1912–1929.
Douillet, G., Rasmussen, K.R., Kueppers, U., Castro, D., Merrison, J.P., Iversen, J.J., Dingwell, D.B., 2014. Saltation threshold for pyroclasts at various bedslopes: wind tunnel measurements. J. Volcanol. Geotherm. Res. 278–279, 14–24.

Gillies, J.A., Nicking, W.G., Tilson, M., Furtak-Cole, E., 2012. Wind-formed gravel bed forms, Wright Valley, Antarctica. J. Geophys. Res. 117. http://dx.doi.org/10.1029/2012JF002378.

Golombek, M., Robinson, K., McEwen, A., Bridges, N., Ivanov, B., Tornabene, L., Sullivan, R., 2010. Constraints on ripple migration at Meridiani Planum from Opportunity and HiRISE observations of fresh crater. J. Geophys. Res. 115. http://dx.doi.org/10.1029/2010JE003628.

Greeley, R., Iversen, J.D., 1985. Wind as a Geological Process. Cambridge Univ. Press, Cambridge, UK, 333 p.

Iversen, J.D., White, B.R., 1982. Saltation threshold on Earth, Mars, and Venus. Sedimentology 29, 111–119.

Iversen, J.D., Pollack, J.B., Greeley, R., White, B.R., 1976. Saltation threshold on Mars: the effect of interparticle force, surface roughness, and low atmospheric density. Icarus 29, 381–393.

Kok, J.F., 2010. Difference in the wind speeds required for initiation versus continuation of sand transport on Mars: implications for dunes and dust storms. Phys. Rev. Lett. 104, 074502.

Kok, J.F., Parteli, E.J.R., Michaels, T.I., Bou Karam, D., 2012. The physics of wind-blown sand and dust. Rep. Prog. Phys. 75, 106901.

Mandt, K., de Silva, S.L., Zimbelman, J.R., Crown, D.A., 2008. The origin of the Medusae Fossae Formation, Mars: insights from a synoptic approach. J. Geophys. Res. 113. http://dx.doi.org/10.1029/2008JE003076.

Mandt, K., de Silva, S.L., Zimbelman, J.R., Wyrick, D., 2009. Distinct erosional progressions in the Medusae Fossae Formation, Mars, indicate contrasting environmental conditions. Icarus 204, 471–477.

Milana, J.P., 2009. Largest wind ripples on Earth? Geology 37, 343–346.

Milana, J.P., Forman, S., Krohling, D., 2010. The largest ripples on Earth: reply. Geology 38, e219–e220.

Montgomery, D.R., Bandfield, J.L., Becker, S.K., 2012. Periodic bedrock ridges on Mars. J. Geophys. Res. 117. http://dx.doi.org/10.1029/2011JE003970.

Moore, H.J., 1985. The Martian dust storm of Sol 1742. J. Geophys. Res. 90, D163–D174.

Scott, D.H., Tanaka, K.L., 1982. Ignimbrites of the Amazonis Planitia region of Mars. J. Geophys. Res. 87, 1179–1190.

Squyres, S.W. et al., 2004. In situ evidence for an ancient aqueous environment at Meridiani Planum, Mars. Science 306, 1709–1714.

Sullivan, R. et al., 2005. Aeolian processes at the Mars Exploration Rover Meridiani Planum landing site. Nature 436. http://dx.doi.org/10.1038/nature03641.

Ungar, J.E., Haff, P.K., 1987. Steady-state saltation in air. Sedimentology 34, 289–299.

Weitz, C.M. et al., 2006. Soil grain analyses at Meridian Planum, Mars. J. Geophys. Res. 111. http://dx.doi.org/10.1029/2005JE002541.

White, B.R., 1986. Particle dynamics in two-phase flows. In: Encyclopedia of Fluid Mechanics. Gulf Publishing Company, Houston, TX (Chapter 8).

White, B.R. et al., 1976. Estimated grain saltation in a Martian atmosphere. J. Geophys. Res. 81, 5643–5650.

Yizhaq, H., Kok, J.G., Katra, I., 2014. Basaltic sand ripples of Eagle Crater as indirect evidence for the hysteresis effect in Martian saltation. Icarus 230, 143–150. http://dx.doi.org/10.1016/j.icarus.2013.08.006.

Zimbelman, J.R., 2010. Transverse aeolian ridges on Mars: first result from HiRISE images. Geomorphology 121, 22–29.

Zimbelman, J.R., Scheidt, S.P., de Silva, S.L., Bridges, N.T. Spagnuolo, M.G., 2014. Roughness height measurements for megaripples in the Puna of Argentina, form flow over the largest megaripples and implications for Mars. In: Lun. Planet. Sci., XLV, 1359.